

# Düzce University Journal of Science & Technology

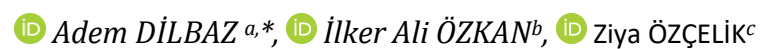


https://dergipark.org.tr/tr/pub/dubited



Research paper

# Simulation-Based Optimization of Robotic Weld Seam Tracking Using Fuzzy C-Means Clustering and PID Control



- <sup>a</sup> Selçuk University, Institute of Sciences, Department of Mechatronics Engineering, Konya, Türkiye.
- <sup>b</sup> Selçuk University, Faculty of Technology, Department of Computer Engineering, Konya, Türkiye.
- <sup>c</sup> Selçuk University, Faculty of Technology, Department of Mechatronics Engineering, Konya, Türkiye.
- \*Corresponding author: ademdilbaz25@gmail.com

#### Article information:

Received: 24/06/2025, Revision: 30/08/2025, Accepted: 29/09/2025

DOI: 10.29130/dubited.1724335

#### **ABSTRACT**

Today, welding automation is a vital technology that boosts efficiency in manufacturing processes while enhancing weld quality by minimizing human intervention. However, deformations caused by high heat and deviations from programming errors in robotic welding can negatively impact welding quality. Existing camera and laser-based seam tracking systems are insufficient in certain scenarios due to factors such as highly reflective surfaces, intense arc radiation, or uneven surface conditions. This article presents a weld seam tracking system based on an angle sensor, called Weld Guide, developed to address the limitations of existing systems. The proposed system features angle sensors that utilize a Contact-based sensor principle to improve the accuracy of the robotic welding torch. The Weld Guide system was designed using SolidWorks software, simulated in RoboDK simulation software, and validated through experimental tests. The prototype was tested on both linear and curved weld seams, and its performance under different control systems was evaluated using an optical microscope. Results from the experiments showed that the Weld Guide system successfully tracked weld seams with a deviation of less than 0.6 mm. The comparison between the trajectories obtained from simulated and actual field tests exhibited a similarity exceeding 97%, demonstrating a high level of accuracy in trajectory-tracking performance. Furthermore, a hybrid approach combining Fuzzy C-Means (FCM) clustering with Proportional Integral Derivative (PID) control was implemented to enable automatic tuning of the PID parameters. By incorporating oscillation levels into the fuzzy logic rules, the optimization was enhanced against sudden changes, thereby preventing error accumulation and excessive oscillations. These findings indicate that the proposed system provides a reliable and cost-effective alternative when optical-based tracking methods fall short.

**Keywords:** Angle Sensors, Contact-Based Sensor, FCM-PID, Robodk, Robotic Welding, Simulation, Solidworks, Weld Seam Tracking

#### I. INTRODUCTION

Robots are systems that perform specific tasks by operating their mechanical components based on preprogrammed commands. Robotic manufacturing is typically carried out in industrial production processes using devices that can be programmed to operate without human intervention (Wang et al., 2020). Previous research has shown that robotics is effectively utilized in various areas of manufacturing. Robotic welding processes are among the most widely preferred applications (Ramalingam et al., 2021). Furthermore, in

robotic welding, the high quality and precision of automatic seams stand out in comparison to traditional methods.

Nowadays, robotic systems are integrated into welding seam processes to be automated. A weld bead is a joining process in which one or more workpieces are fused by applying heat, pressure, or both, with or without the use of filler material, in continuous or intermittent welding (Li et al., 2020). In welding manufacturing, robotic systems bring significant advantages in terms of precision and labor costs during the production process compared to manual methods (Sharma et al., 2020). Moreover, the concept of seam welding has improved in recent years, and researchers have used various auxiliary techniques for this purpose (Reddy et al., 2024). Robotic welding seams occasionally carry the risk of errors due to various disruptive external factors. In some applied research and projects that aim to eliminate such errors, camera, laser, or arc sensor-based systems are commonly used.

For weld seam tracking, much research has been carried out primarily on camera systems due to their more economical and simple structure. In a study, an experiment was set up using a camera to detect the area to be filled with weld, and it was aimed to learn whether instability can occur in noisy environments (Xue et al., 2021). However, it was determined that not only the camera system is insufficient, but the laser system should also be present. In another study, a test setup was designed to evaluate weld seam tracking under noisy welding conditions. The experiments revealed that strong arc radiation and spatter significantly degraded the image quality, making seam tracking challenging (Liu et al., 2018). Similar studies in the literature reveal the limitations of camera systems in weld seam tracking (Zou et al., 2020; Yang et al., 2020). Therefore, to achieve more reliable and high-precision weld seam tracking, alternative systems to camera systems have been explored, leading to investigations of laser systems. The measurement accuracy of laser area scanning systems, which have recently gained popularity, varies depending on the type and power of the beam and the software costs. The reflection or absorption of the laser beam is utilized to determine the position and shape of the seam. These systems are ideal for remote sensing since they can project a narrow beam over long distances. Operating in three dimensions, laser seam tracking sensors generally scan within periods of tens of arc seconds. The operational principles of the laser system are illustrated in detail in Figure 1. During the operation of these sensors, results are obtained based on one or more laser beams that leave a device, hit the surface (X), reflect off it, and return to the camera (Y). Thus, the laser beams emitted from the diode and those captured by a filtered image sensor are compared through trigonometric operations.

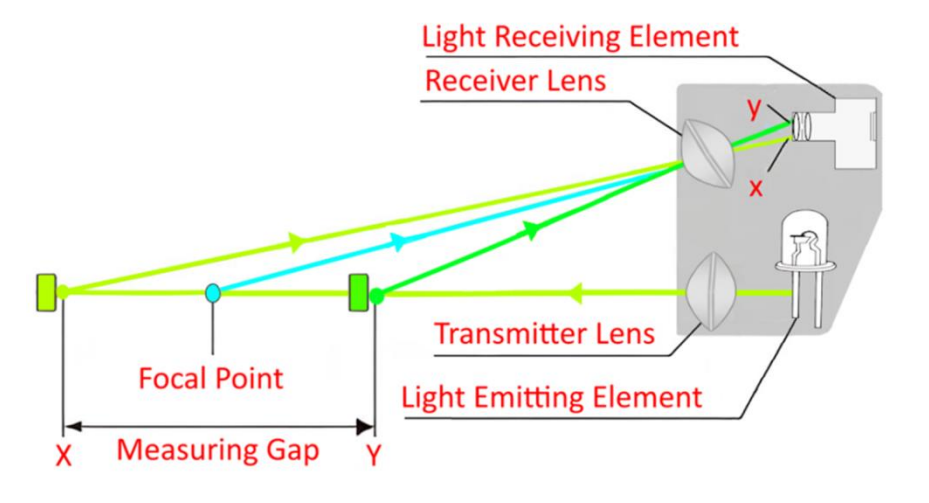


Figure 1. Working principle of laser Seam Tracking system

Thermal deformation is a distortion that causes a material to change shape or size when subjected to temperature changes. This problem is a result of the coefficient of thermal expansion or contraction of a welded material. These distortions have been observed more frequently in long-distance or high-amperage welding processes, especially in materials with a thickness of 6 mm or less (Nguyen & Lee, 2014).

While laser sensors have many advantages, they also have some disadvantages such as complexity in parameterization and steam up of the lens. In a study conducted on these disadvantages, various problems related to the protective glass of the lens for the laser sensor, which is an expensive system, were examined

(Suoranta, 2021). In another study, the protective glass in front of the lenses has caused destructive effects in some measurements by creating internal reflections (Skála et al., 2016). In addition to this, dust particles on the protective glass could reduce the clarity of the received data. In a sample study, the data obtained in the measurement of surface roughness for sample materials with a glossy surface were plotted. However, the results obtained in a non-contact way for samples with high surface reflections were not accurate enough, so it was recommended that the laser sensor should not be used for materials with glossy surfaces (Cibicik et al., 2021).

In addition to laser sensors, tactile arc sensors are also used for weld seam tracking. These sensors are preferred for seam tracking in t and inner fillet welding applications. These sensors, which obtain voltage measurements by touching the wire at the tip of the torch to the edges along the weld seam, help the torch to provide weld seam tracking (Ružbarský, 2023). However, these sensors cannot be used in submerged arc welding applications due to inaccurate measurements when the wire at the tip of the torch contacts dust grains. In addition, fractures can also occur in spot welds applied to prepare workpieces for the process due to high-temperature shrinkage. As a result, the weld gap may widen more than it should, and the welding process may fail due to insufficient penetration into the gap.

In welding processes, seam tracking improves the quality of the process by adjusting the free wire length (CTWD) appropriately. The wire length here is the remaining part between the length of the protruding wire at the tip of the torch and the arc length. If the appropriate wire length cannot be adjusted, the peeling strength, which protects the weld in the material against cracking, may also decrease. This peeling strength is directly proportional to the average load per unit width required to separate the materials that will be joined. The amount of load here is a very important criterion that determines the durability of a welded joint. In an experimental study conducted for gas metal arc welding, it was aimed to determine that the peeling strength decreases with the increase in free wire length (Petschnigg et al., 2018). This is because of that the formation of the weld pool by spraying molten metal from a great distance reduces the penetration and weakens the mechanical strength of the welding seam. In another experimental study on gas metal arc welding, it was determined that when the distance from the torch to the workpiece is more than 35 mm from the first welding pass, the weld thickness appears smaller than it should be (Lu et al., 2015).

In another study conducted on the use of angle sensors in weld seam tracking, the height adjustment to prevent the torch from hitting the ground was tested. In this study, an experimental setup was prepared to follow the weld gap of 4 mm width and 2-6 mm depth curvilinearly for 260 mm. In this setup, changes in the weld gap depth were successfully detected thanks to the angle sensor setup (Seefried et al., 2021). In a study in the literature, studies were conducted on the use of angle sensors together with laser sensors in corner weld seams of concrete piles with X-shaped ends. Since the positions of the materials here can change in some processes, the developed weld seam tracking system was used and positive results were obtained (Huynh & Phung, 2024).

In robotic weld seam tracking, laser, and camera-based systems are negatively affected by some factors such as shiny surfaces or high arc radiation. In addition, the inaccurate measurements of arc sensors in submerged arc welding applications demonstrate that current systems cannot provide reliable results in certain welding environments. Therefore, heat-induced deformations and weld seam deviations cannot be adequately detected by current methods. These mentioned major problems highlight the need for a more reliable and accurate system for robotic weld seam tracking. In this paper, the proposed system detects deviations that may occur during the weld seam and adaptively updates the PID parameters based on the dynamic states of the servo motors using the FCM-PID algorithm, enabling precise and stable motion of the robot along the Cartesian axes. While laser-based methods are commonly employed in the literature for such problems, this study presents a touch-based approach. Laser systems are generally positioned 70–100 mm ahead of the torch, whereas the proposed system moves in alignment with the welding torch, offering a more reliable and effective solution for applications where collision risks exist. Additionally, due to its touch-based nature, the system can operate both independently and in integration with laser systems under harsh environmental conditions such as reflection, rust, and stray emissions, thereby providing valuable contributions to the literature. Moreover, among the existing methods are arc sensors and camera-based systems. However, since welding weaving is not applied in some welding processes. Arc sensors cannot be effectively employed, as they require a minimum weaving motion of 1 mm, which is not present in certain welding processes. In contrast, the system developed within the scope of a doctoral dissertation, named Weld Guide, which is capable of performing measurements without weaving, can determine the weld seam tracking point through contact with the workpiece edges. In addition, camera-based systems are adversely affected by the high light intensity and metal spatter generated during welding, whereas the Weld Guide system, which does not include optical components, is able to achieve micron-level weld seam tracking even under disruptive environmental conditions.

During the design phase of the Weld Guide system, factors such as precision, stability, fast response, and compatibility were taken into consideration. Furthermore, the innovative experimental setup to be developed, which is based on a hybrid approach combining Fuzzy C-Means (FCM) clustering and PID control, is expected to provide an additional solution to existing sensor systems and make a significant contribution to the literature in the field of weld seam tracking. In a related study, the variability of equivalent inertia and gravity applied to the servo motor shafts posed challenges for achieving satisfactory control performance using a conventional PID controller (Han et al., 2023). To address this issue, the effects of dynamic characteristics on control performance were analyzed. A clustering algorithm combined with fuzzy logic was then employed to extract control parameters in real time, resulting in improved optimization.

Fuzzy logic addresses the limitations of classical control by modeling nonlinear system behaviors through membership functions and fuzzy rules. The FCM-based control architecture was able to achieve high performance across a broader operating range by adapting to the system's dynamics through fuzzy rules and continuously updating its membership functions based on real-time data (Behrooz et al., 2019). As a result, the control system can effectively manage nonlinear and time-dependent scenarios, such as oscillations, and unexpected external disturbances. In addition, rapid adjustments of PID parameters can lead to undesired oscillations and overshoot in the control system; therefore, the rate of parameter changes can be constrained using a Fuzzy C-Means-based adaptive mechanism that operates over clusters with predefined boundaries (Ferdaus et al., 2019).

The rest of this paper is organized as follows: Section 2 describes the experimental design and development of the sensing system, including the methods used. Section 3 presents the simulation and reality testing results and comparative analysis. Finally, Section 4 reviews the results, highlights the contributions of the study, and suggests potential areas for future research.

#### II. MATERIAL AND METHOD

The developed system addresses a new experimental setup for robotic welding seam tracking to overcome the limitations of existing sensor systems. Designed to detect deformations and seam deviations during the welding process with high accuracy, this system is compatible with Metal Inert Gas(MIG), Metal Active Gas (MAG), and Submerged Arc Welding (SAW) applications. The proposed experimental setup provides real-time feedback based on contact measurements and is designed for integration with existing sensor systems. In this context, the sensors, mechanical components, and software-assisted analysis methods used during the design phase of the experimental setup are discussed in greater detail. This section will first explain the design process of the experimental setup and the components used, then test the system's performance and explain how the obtained data is processed. Finally, simulation analysis using RoboDK software will be presented.

# A. Design Process of the Experimental Setup

In the first stage of the experimental work, the design of the experimental setup suitable for both gas and submerged arc applications in weld seam tracking was initiated. This design is intended to support developments in industrial production processes and integrate with existing auxiliary systems. Consequently, it will be possible to address areas where current auxiliary systems fall short in weld seam tracking processes. In this regard, mechanisms were developed during the design process that can perform weld seam tracking with precision and enhance the system's accuracy. The design steps of these mechanisms and the components used are discussed in detail below.

In the design process of the experimental setup, two independent mechanisms were created that can make measurements and detect angular changes by contacting the surfaces on the workpiece. The connections of these mechanisms were made with knuckle joints and fixed to the neck of the welding torch with a fiber wood clamp through other joints. The joints were equipped with angle sensors and the sensor and clamp materials were selected from metal materials that are resistant to environmental factors such as high heat, fire spatter, and burr adhesion in the welding zone.

The basic procedures applied in the design of the experimental setup can be summarized as follows:

- The RCB 3100 series angle sensor has a measurement capacity of 120° that can mechanically rotate to 124° and can be stopped at the borders with supports. It was possible to design a joint to connect this sensor to the experimental setup through the assembly holes in its body.
- The clamp part is made of fiber wood with a 0.05 mm grip gap and is designed to be easily mounted on the neck of a 25 mm diameter welding torch.
- The probe arm was custom-fabricated by adapting a 7 mm Allen key, allowing precise integration with the short arm of the angle sensor. This allowed the design to be completed with a 0.02 mm space for assembly.

#### B. Testing and Validation

SolidWorks software was used for the design verification, component compatibility check, and assembly simulations of the Weld Guide experimental setup. This software allows the precise positioning of components through its three-dimensional modeling and virtual assembly capabilities. In this program, analog output angle sensors and probes with spring mechanisms that detect angular changes when the welding torch approaches or moves away from the edge surfaces of the workpieces to be welded are modeled. Figure 2 details the components of the system and the layout of these sensors.

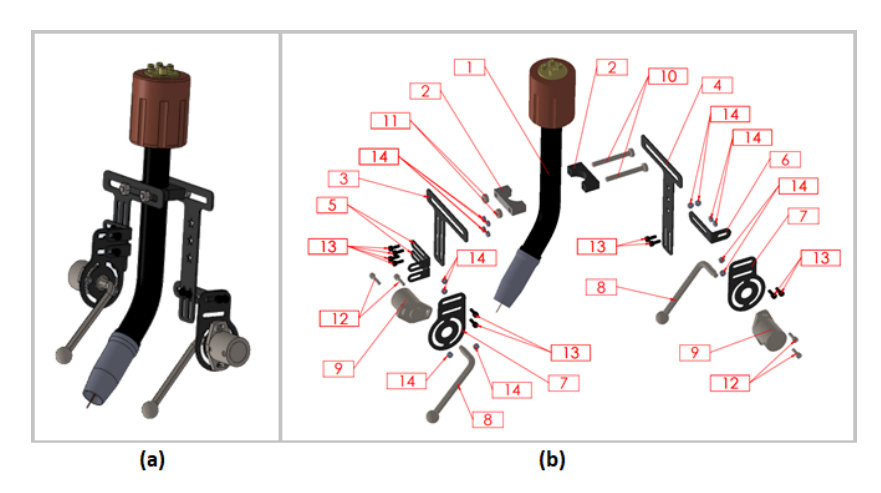


Figure 2. (a) Weld Guide system with welding torch assembly visual, and (b) exploded view with details

The designs of all parts in the Weld Guide experimental setup were successfully assembled using the SolidWorks program, as shown in Figure 2(a). Figure 2(b) shows the exploded assembly visualization, which provides a more detailed view of the experimental setup. This image clearly shows how the components are integrated and the structural position of each part. In this way, the pre-assembly positioning of the angle sensors and sensor arms used in the system is shown in detail, emphasizing the functional integration of the components. These L-shaped arms are designed for a tight connection to the D-shaped housing of the sensor swivel joint.

In Figure 2(b), which is a detailed view of the Weld Guide system, part number 8 represents the sensor probe arm. The tip of this probe arm is in direct contact with the surface of the workpiece during the welding process to detect angular changes. In order to increase the wear resistance of the component in contact with the surface, heat-treated high-carbon steel balls were used for the end of the sensor probe arm. These steel balls, which are heat-treated to an average hardness of 60 HRC, can harden further under high temperatures and mechanical load. However, this hardening also increases the brittleness of the material, leading to the risk of cracking (Budde et al., 2023). To solve the joining problem of this material, laser welding was used, and it successfully joined another steel with suitable parameters thanks to its narrow heat input and high precision. ST37 steel is generally considered equivalent to the European standard S235JR, with a hardness level of approximately 16-20 HRC In contrast, ST52 steel has a higher yield and tensile strength and is classified as a harder and stronger material mechanically (Haeri et al., 2024).

In the Weld Guide system, the rotary joint part of the angle sensor is designed based on the coil spring mechanism. This spring mechanism works by storing energy in the angular direction and rotating one of the spring arms around its body. In this way, the spring can store the force applied in the direction of rotation and act as a means of moving the sensor probe arm in the opposite direction. Thus, this arm, which moves clockwise, can automatically return counterclockwise due to the spring mechanism.

Table 1. Material properties and weight distribution of components in the Weld Guide experimental setup

Material	Number	Material Type	Quantity(pcs)	Weight
Wood fibre clamp	2	Plywood	2	21.98
Joint A	3	S235JR steel	1	37.96
Joint B	4	S235JR steel	1	55.69
Joint C	5	S235JR steel	2	9.49
Joint D	6	S235JR steel	1	14.69
Joint E	7	S235JR steel	2	34.58
Sensor probe	8	Chrome vanadium nickel	2	43.71
Angle sensor	9	Aluminum	2	119.12
M6 screw	10	Stainless steel	2	14.05
M6 nut	11	Stainless steel	2	2.79
M4 screw 15 mm	12	Stainless steel	4	2.23
M4 screw 10 mm	13	Stainless steel	10	2.03
M4 nut	14	Stainless steel	14	0.80
Joint reinforcement	(*)	Stainless Steel	1	48.80

**Notes:** The total weight of all parts in the experimental setup is 706.15 g (\*) Joint reinforcement was introduced after field testing to enhance structural stability and reduce

potential misalignment.

The primary component that connects the Weld Guide experimental setup to the welding torch as an insulator is the clamp, which is constructed from wood fiber material divided into two sections. This material boasts a high screw-holding capacity and ensures safe usage in fiery environments by maintaining its structural integrity even when exposed to burning spatter (Costa et al., 2018). The component that links this clamp to the first angle sensor sensing system and facilitates linear positioning is Joint A. Similarly, Joint B connects the clamp to the second angle sensor sensing system and provides linear positioning. The upper section of the Weld Guide experimental setup is comprised of these three parts. A detailed view of all components in this system is presented in Figure 2. Weight information, material names, and types for these parts, listed in numerical order, are available in Table 1.

## C. Mathematical Modeling and Data Analysis

In robotic welding applications, precise control of the end-effector position in a three-dimensional coordinate system is critical to obtain high-quality welds and minimize errors. The Tool Center Point (TCP) is a critical reference point that ensures the positioning accuracy of the robot arm. In welding operations, a correct TCP calibration enables the weld path to be followed as desired and prevents weld errors. In a study conducted on this position, called the contact point in welding applications, tests were conducted on using this center coordinate information to learn the Cartesian positions of the axes in the robotic arm (Bryn et al., 2016). In another study based on previous studies on the trajectory estimation of Cartesian axis points, tests were conducted on the ability of the welding robot to move linearly in the X, Y and Z axes with a ball screw-shaft actuator mechanism and stepper motors driven by the body part. In these tests, by using TCP coordinates, it was observed that the robot could perform welding applications within the work area with Cartesian movements, and these linear movements were defined as PPP (Prismatic, Prismatic, Prismatic) type (Huang et al., 2020). This structure enables precise positioning of the welding torch by allowing the end effector to move linearly in three axes.

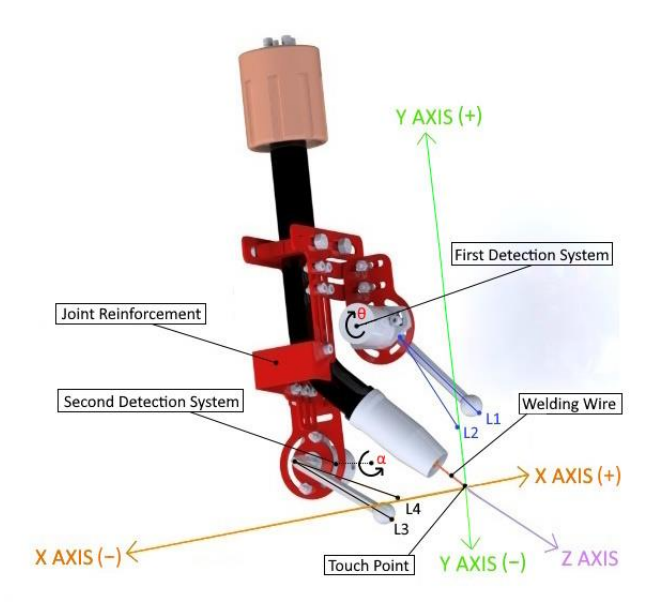


Figure 3. Detection systems on Weld Guide experimental setup

Two RCB 3100 angle sensors were used in the Weld Guide experimental setup. When the datasheets of these sensors are examined, it is understood that they perform their measurements with an error margin of  $\pm$  0.5%. Figure 3 shows the positioning of the sensing systems in the Weld Guide experimental setup. In this figure, the Z axis represents the robot's route on the weld seam path. The first sensing system detects angular changes based on the change in position of the Touch Point on the Y-axis, while the second sensing system calculates angular changes based on the change in position on the X-axis. These sensors optimize the robot's position values by periodically analyzing the extreme position of the welding wire.

In a study, it was assumed that the associated load and arm motion are represented as a compound pendulum by adopting a mathematical procedure (Soltani & Vahidi, 2024). In another study, tests were performed on pendulum-driven spherical mobile robots with limited partial lateral mobility. In these tests, position and orientation values could be determined based on the changes of  $\theta$  angle values in pendulum-driven rotations with non-zero minimum turning radius (Ibrahim & Al Akkad, 2017). The two sensor probe arms used in the Weld Guide were experimental setup have different lengths. These probe arms move clockwise and counterclockwise to determine the coordinates of the points contacting the workpiece in the X and Y axes. In previous studies, it was reported that the right triangle theorem was utilized to determine the projection distances of the contact points in the X and Y axes in such mechanisms (Zhang et al., 2021). Similarly, in this study, using the sine and cosine theorems, the amount of deviation of the welding torch from seam tracking is mathematically formulated as a function of the angular variations at the first and second contact points.

To ensure precise measurements, the installation angles of the probe arms were set to  $45^{\circ}$  for the X and Y axes to achieve maximum accuracy. The length of the probe arms in the angle sensors was determined as L1 = 92 mm and L3 = 87 mm based on the measurements. As shown in Figure 3, the amount of error (LX) in the X axis when the L1 deflection point is reached from the L2 contact point, the perpendicular projections of the L2 and L1 points on the X axis (L2X and L1X) are calculated as follows:

$$L1_{X} = L1\cos(45) \tag{1}$$

$$L2_X = L1\cos(45 + \theta) \tag{2}$$

$$L_X = 92 (\cos (45) - \cos (45 + \theta)) \tag{3}$$

In Eq. 3. the probe arm of the first angle sensor with length L1 is positioned at a 45° angle to the ground in the set configuration. Subsequently, this angle value varies according to the deviation along the X-axis, and the corresponding deviation amount is obtained as LX, as shown in Figure 3. Similarly, when the deviation point L3 is reached from the contact point L4 in Figure 3, the amount of error on the Y axis (LY) is calculated as the perpendicular projections of the points L4 and L3 on the Y axis (L4Y and L3Y) as follows:

$$L3_{Y} = L3\cos(45) \tag{4}$$

$$L4_Y = L3\cos(45 + \alpha) \tag{5}$$

$$L_Y = 87(\cos(45) - \cos(45 + \alpha)) \tag{6}$$

In Eq. 6. the probe arm of the second angle sensor with length L2 is positioned at a 45° angle to the ground in the set configuration. Subsequently, this angle value varies according to the deviation along the Y-axis, and the corresponding deviation amount is obtained as LY, as shown in Figure 3. These formulas determine the amount of deflection of the welding torch and ensure the accuracy of the system. The angle sensors used in the experimental setup determine the amount of deflection in line with these calculations and provide real-time correction data.

The output signal of each angle sensor in the Weld Guide experimental setup varies between  $0.5-4.5 \, \text{V}$  DC (Direct Current). However, these sensors can give an output signal between  $2^{\circ}$  and  $120^{\circ}$  degrees. In addition, the rotation degrees are mechanically limited after  $124^{\circ}$  and it is not possible to perform more rotations. In this study, the voltage value obtained from the 1st angle sensor is considered as V1, and the voltage value obtained from the 2nd angle sensor is considered as V2. These voltage values are converted into a variable digital signal with Analog Digital Converters (ADC). In this process, the ADC reference voltage value of the microcontroller used in the system is accepted as  $5 \, \text{V}$ . The values obtained during digital conversion are converted into digital signals by rounding to the nearest integer, as denoted by the symbol []. Taking the number of resolution bits of the ADC as N, the general formula for converting the analog signal  $V_i$  into digital data  $D_i$  according to a fixed reference voltage is given below:

$$D_i = \left[ \frac{V_i - 0.5}{V_{ref} - 0.5} \left( 2^N - 1 \right) \right], i = 1, 2, V_{ref} = 5$$
(7)

In Eq. 7. analog signals in the system were converted into digital data. In this Eq., the value of N corresponds to the resolution of the angle sensor, which is 12 bits. According to this Eq., digital values ranging from 205 to 1842 were obtained from the angle sensor based on its 0.5–4.5 V analog output signal and then processed to be approprate for the robot controller. Thanks to this digital data, the robot controller can evaluate the measured angle changes and make the necessary corrections in the welding process. The set value refers to the predefined reference point for a given system. When the welding torch reaches the seam, the digital data previously obtained when the probe arm of the 1st angle sensor is at position L2, as shown in Figure 3, represents the first reference value. Similarly, the digital data measured with the probe arm of the 2nd angle sensor at position L4 represents the second reference value. By comparing these reference values with the instantaneously measured digital data, the amount of error is calculated, and necessary corrective actions are taken by the robot controller.

By incorporating the position-deviation data acquired from the sensors expressed in millimeters as the  $p_x$ ,  $p_y$ , and  $p_z$  components of the translation vector in the homogeneous transformation matrix, the joint angles of the six-axis robot can be computed with high accuracy.

$$T_i = \begin{bmatrix} R_i & t_i \\ 0 & 1 \end{bmatrix} = \begin{bmatrix} p_x \\ R_i & p_y \\ p_z \\ 0 & 1 \end{bmatrix}$$
 (8)

In six-axis robotic welding, the 5th, and 6th axes are generally kept fixed. For example, this condition is utilized as a TCP point teaching function in CLOSS Qineo ArcBot systems. This information is also documented in the CLOOS Welding Robots and Machines Seminar Catalog, providing additional technical reference on the subject. Since field operations will also involve applications requiring this feature, the last three axes of the six-axis robot—namely, the roll, pitch, and yaw axes—will remain fixed. Consequently, optimizations will focus solely on the adjustment of the  $\theta_1$ ,  $\theta_2$ , and  $\theta_3$  joint angles. In this context, based on the changes observed in the TCP positions, it is possible to calculate the variations in these joint angles using inverse kinematic equations. In a similar study in the literature, it has been possible to determine the joint values from the TCP positions and orientation information of the robot, with only touch-up or calibration processes remaining for certain positions (Vacharakornrawut et al., 2016).

Using the Denavit–Hartenberg (DH) parameters, a transformation matrix is generated for each joint. By multiplying these matrices, the position and orientation (x, y, z, roll, pitch, yaw) of the end effector TCP can be computed. In a study from the literature, the overall deviations of the TCP, calculated from the D-H

parameters, have been successfully obtained (Vocetka et al., 2020). Using inverse kinematic equations, the calculations demonstrating the values of  $\theta$ , and are presented below. In the CLOOS robot QIROX software, the values indicated for TCP positions are converted to millimeters by multiplying by 1/10. This conversion has been taken into account in the presented calculations. In this study, the 1st, 2nd, 3rd and 4th axes are active while the 5th, and 6th axes remain fixed. In this context, the resulting  $\theta$  values have been obtained based on the formulas derived for a 6-degree-of-freedom (DoF) Euler wrist robot arm (Hong et al., 2018).

$$\begin{cases} \theta_{1} = atan2 \left(-p_{x}, p_{y}\right) \mp atan2 \left(p_{x}^{2} + p_{y}^{2} - d_{2}^{2}, d_{2}\right) \\ \theta_{3} = atan2 \left(\frac{-p_{x}^{2} + p_{y}^{2} + \left(p_{z} - l_{1}\right)^{2} - l_{4}^{2} - l_{2}^{2} - d_{2}^{2}}{2 l_{4} l_{2}}, \mp \sqrt{1 - \left(\frac{p_{x}^{2} + p_{y}^{2} + \left(p_{z} - l_{1}\right)^{2} - l_{4}^{2} - l_{2}^{2} - d_{2}^{2}}{2 l_{4} l_{2}}}\right)^{2} \right) \\ \theta_{2} = atan2 \left(l_{4} \sin \theta_{r3} - l_{2}, -l_{r4} \cos \theta_{r3}\right) \mp atan2 \left(\sqrt{l_{4}^{2} + l_{2}^{2} - 2 l_{2} l_{4} \sin \theta_{3} - \left(p_{z} - l_{r1}\right)^{2}}, p_{z} - l_{r1}\right) \\ \theta_{4} = -arctan \left(\pm \left(p_{z} - l_{3} \sin \theta_{3} - d_{2} \sin \theta_{1} - l_{2} \cos \theta_{2}\right), \pm p_{y}\right) \\ \theta_{5} = arctan \left(p_{x} - l_{2} \cos \theta_{2} - l_{3} \cos \theta_{3}, \pm \left(\sqrt{\left(l_{6} \cos \theta_{6}\right)^{2} - \left(l_{1} \sin \theta_{1} + l_{3} \cos \theta_{3} - p_{x}\right)^{2}}\right) \\ \theta_{6} = arctan \left(l_{3} \sin \theta_{3} + l_{4} \sin \theta_{4} + l_{2} \cos \theta_{2} - p_{z}, p_{y}\right) \end{cases}$$

$$(10)$$

It is clear from Eq. 9. the solution of inverse kinematics, depending on the geometrical approach, is complex and more cumbersome (Sharkawy & Khairullah, 2023). In the first part of the Eq. 9., it provides the variation values of the angle  $\theta_1$  in the range  $[-\pi, \pi]$ , taking into account the changes in the X and Y TCP coordinates along the weld seam. In the second part of this Eq. 9., the  $\theta_2$  angle is determined using the atan2 function, which determines the correct quadrant of the X and Y TCP coordinates within the range  $[-\pi/2, 5\pi/3]$ . The four quadrants are defined as: X>0, Y>0; X>0, Y<0; X<0, Y>0; X<0, Y<0. In the third part of this Eq. 9., the  $\theta_3$  angle is determined using the atan2 function which determines the correct quadrant of the X and Y TCP coordinates within the range  $[-3\pi/4, 5\pi/6]$ . In this context, l2 represents link length, while the others (l1,l3, and d2) represent link offset. These values were obtained from the technical drawings of the Qirox robot as  $l_1 = 457$  mm,  $l_2 = 651$  mm, and  $l_3 = 767$  mm,  $d_2 = 268$  mm respectively.

Considering the  $\alpha$  and  $\theta$  values obtained from the angle sensors in the Weld Guide experimental setup, the amount of error on the X and Y axis when the deviation point is reached can be obtained by Eq. 3. and 6.. In addition, the instantaneous angle information according to the voltage value read from each angle sensor can be obtained using Eq. 7.. The algorithm showing the working principle of the experimental setup is presented in Figure 4. According to the algorithm, four different output data are generated using two different input data. These outputs represent the linear movements of the robot along the X(+), X(-), Y(+) and Y(-) axes. This allows the robot arm to perform Cartesian motions along the X(+), X(-), Y(+), Y(-), Z(+) or Z(-) axes. The robot achieves precise positioning and mobility through six-axis rotational motion (Elsisi et al., 2021).

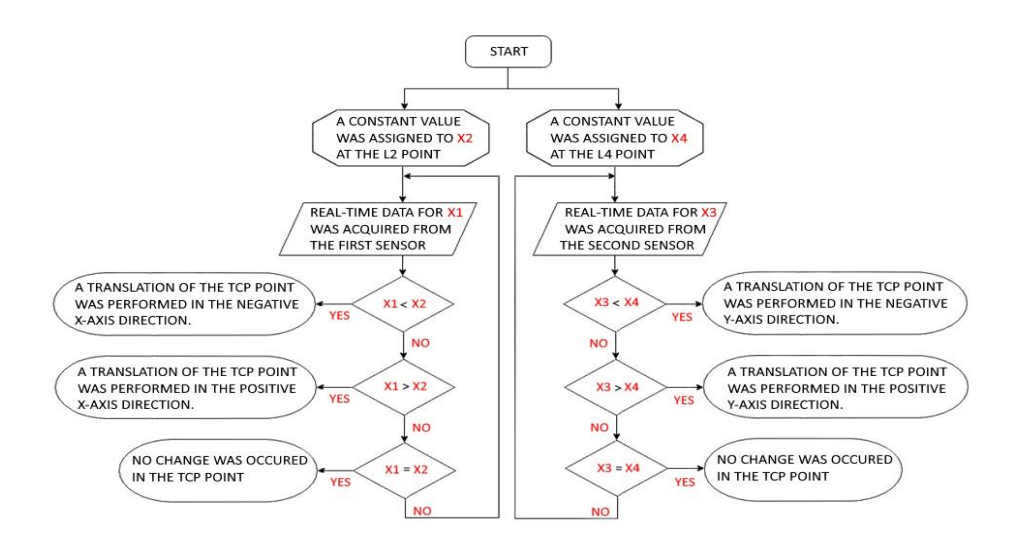


Figure 4. Working principle of the Weld Guide experimental setup

#### D. Simulation-Based Validation of Weld Guide System

Within the scope of this paper, RoboDK simulation software, which is widely used in similar studies, was preferred in order to detect possible errors of the designs before the actual field tests (Henriques et al., 2023). This software is a simulation that can generate code suitable for various types of robots from more than 50 manufacturers and simulate welding, assembly and machining processes (Corke, 2017). This software offers the possibility to perform simulations without stopping the operation of a new robot system to be tested. This program includes an innovative and rich library of programs capable of intuitively obtaining very realistic results (Garbev & Atanassov, 2020).

RoboDK simulation can also provide the possibility to find the joint values of an element corresponding to a certain position and to transform from task space coordinates to joint space coordinates. The Python software codes that can run within this program have an important influence on the choice of simulation program in many academic studies. The Python codes developed on the RoboDK program were successfully tested on a virtual robot thanks to a series of algorithms. Afterwards, these codes could be directly transferred to the controller of a special robot, and the manufacturer-independent programming capability was utilized (Lin et al., 2022). In Morsi's simulation study conducted to prevent collisions and verify the system design using the RoboDK software, the new fork-shaped apparatus was modeled. In this simulation, an HP brand webcam, LED backlighting and inspection camera layout plan were made. According to this plan, the inspection camera was positioned on the right end of the designed apparatus. The simulation tests performed on RoboDK verified the appropriateness of the assembly processes and the accuracy of component positioning in a virtual environment with high precision (Morsi, 2024). Based on the simulation results, placement errors were avoided in the physical assembly process and the risk of the inspection camera breaking during operation was minimized.

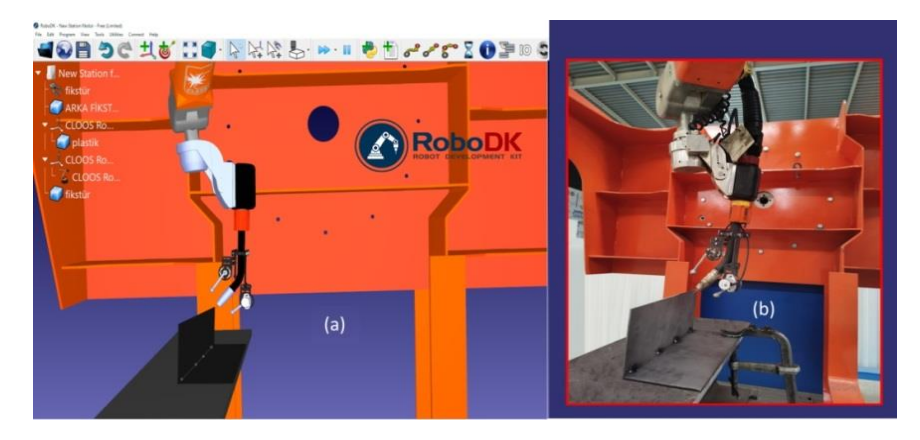


Figure 5. Simulation view of CLOOS robot and photo of Weld Guide experimental setup

In this article, various experiments were continued in the RoboDK simulation environment to further test the applicability of the Weld Guide system in the field. For these simulations, the initial position values of the angle sensors were determined, and the mounting locations of the sensors were adapted to the physical prototype according to these values. As a result of the tests performed in the simulation environment, the response times of the sensors to angle changes were verified before proceeding to field

tests. In line with these findings, it can be concluded that the system satisfies the fundamental requirements prior to field testing, and that an accuracy level suitable for implementation in the physical prototype has been achieved.

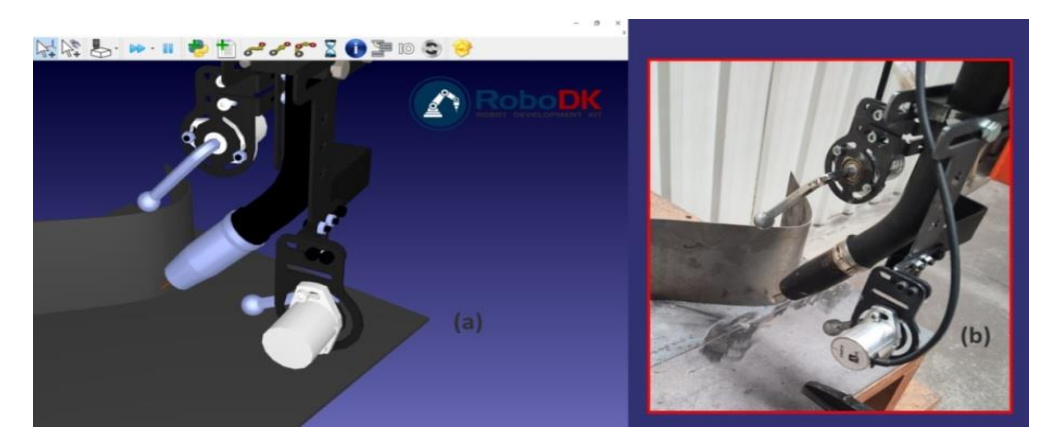


Figure 6. (a) Simulation view of The Weld Guide system detecting a Weld Seam defect in RoboDK environment, and (b) real-time prototype manufacturing scenario showing the defect detection process.

Another experiment with RoboDK was performed with two ST52 steel parts of 250x70x3 mm and 350x350x3 mm thickness joined at an angle of 98 degrees. In the experiment, the simulation image showing the moment of deviation of the robot with the Weld Guide system from the weld seam tracking is given in Figure 6(a). The photograph of the prototype fabrication recorded in the physical environment at the same time is given in Figure 6(b) within the red frame. These images confirm the compatibility between simulation and real tests and show that the system can be successfully implemented in the field.

In another experiment with RoboDK, two pieces of 220x110x3 mm thick ST52 steel were joined at an angle of 81 degrees. In this test run, the initial angle positions of the first and second sensors of the Weld Guide system, which can perform linear weld seam tracking, were not changed. In this case, it was observed that the current positions of the angle sensors were still appropriate in the simulation studies. It was again observed that the experiments performed on the real production and the analyses made in the simulation coincided with each other. The image of the simulation at the moment when the robot with the Weld Guide system continues to follow the weld seam is shown in Figure 7(a), and the photo of the prototype manufacturing at the same time is shown in Figure 7(b) with the red frame. A detailed video recording of this experimental study is available at the link below: <a href="https://youtu.be/9p01fL0H9">https://youtu.be/9p01fL0H9</a> Y

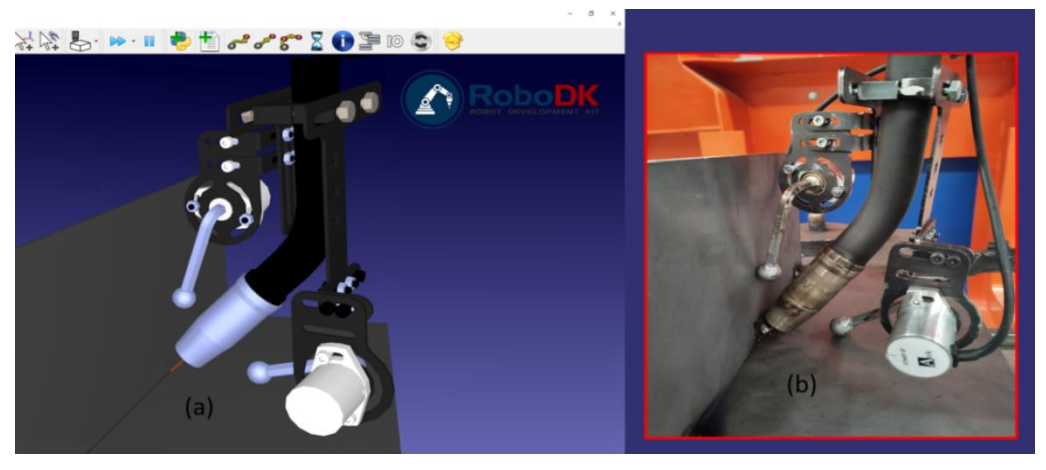


Figure 7. (a) Simulated view of the Weld Guide system during seam tracking, and (b) real-world implementation of the prototype system in actual welding conditions.

In the optimization process, the initial values of the  $K_p$ ,  $K_i$ , and  $K_d$  parameters are set to 8, 0.6, and 0.05, respectively. The robot controller is fundamentally a touch-based Jacobian matrix, which defines the relationship between the motion velocity of the features in the position space and the robot joint angles. In the auto-tuning phase, the incremental PID algorithm is employed, and the digital PID controller can be expressed in discrete time as.

$$\Delta u(k) = K_p(k) z_1(k) + K_i(k) z_2(k) + K_d(k) z_3(k)$$
(11)

The control law is given as (Luo et al., 2022).

$$u(k) = u(k-1) + \Delta u(k) \tag{12}$$

The description of u(k) is the current control output, u(k-1) is the control output from the previous step, and  $\Delta u(k)$  is the amount of change to be applied to the control output in this step. If the error increases,  $\Delta u(k) > 0$ , and the control signal increases, whereas if the error decreases,  $\Delta u(k) < 0$ , and the signal decreases. Where u denotes the output of the PID controller, and k represents the iteration step.

$$\begin{cases}
z_1(k) = e(k) - e(k-1) \\
z_2(k) = e(k) \\
z_3(k) = e(k) - 2e(k-1) + e(k-2)
\end{cases}$$
(13)

The input vectors to be utilized in this context are e(k),  $\Delta e(k)$ , and  $\int e(k)$ . Here, in the vectors, (k) represents the error,  $\Delta(k)$  denotes the error change, and  $\int e(k)$  represents the error integral.

$$\begin{cases} e(k) = r(k) - y(k) \\ \Delta e(k) = e(k) - e(k-1) \\ \int e(k) = \sum_{i=0}^{k} \sum_{i=0}^{k} e(i) \end{cases}$$

$$(14)$$

These vectors will answer the questions of how much the system deviates from the target, whether the error is increasing or decreasing, and whether the error is growing or diminishing. The FCM algorithm defines C clusters. Each cluster has a center  $v_j$  and a membership degree  $\mu_{ij}$  for the input vector. The number of clusters was set to C = 4, corresponding to the fuzzy sets: Big Negative (BN), Small Negative (SN), Small Positive (SP), and Big Positive (BP). These clusters represent variations in linear error and error change, as well as nonlinear oscillation level, thereby characterizing the structure of the fuzzy input data. In particular, the error value, which is the input vector with the highest membership degree and the most significant influence, enabled a faster adjustment of the PID parameters through fuzzy logic; additionally, fine-tuning was completed using the less influential input vectors corresponding to the change in error (Canelas et al., 2018; Chao et al., 2019).

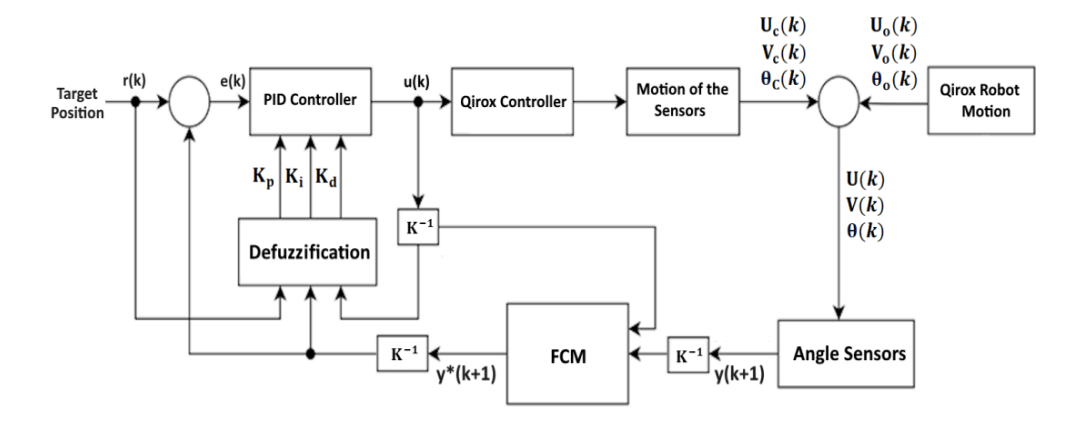


Figure 8. Block diagram of Weld Guide system with FCM-PID controller

To provide a clear understanding of the overall control strategy, the block diagrams of the control loops of the Weld Guide and QIROX systems are shown in Figure 8, illustrating the structure and operation of each

control loop within the respective systems. In this block diagram, the angular sensors provide reference values, and the feedback signals are continuously compared with these references to ensure precise control.

In this study, the membership functions were adjusted to optimize the performance of the PID control system, taking into account similar studies published in the literature,  $\mu_{i1}=0.7$ (error value),  $\mu_{i2}=0.2$ (change of error) and  $\mu_{i3}=0.1$ (oscillation level) that  $\sum_{j=1}^3 \mu ij=1$ . By raising these values to a power (exponentiation), their influence on the fuzzy center is determined. Accordingly, the input vectors are  $x_1$ ,  $x_2$ , and  $x_3$  corresponding to the initial  $K_p$ ,  $K_i$ , and  $K_d$  parameters, respectively. The parameter m (with m > 1) denotes the fuzziness coefficient, which controls the degree of cluster overlap. In alignment with common practice in the literature, m parameter was set to 2 in this study. This parameter plays a critical role in determining the extent of cluster overlap and the overall level of fuzziness (Vesović et al., 2024; Li Sr et al., 2021; Keles et al., 2023). This parameter value choice provides a balanced trade-off between cluster separation and flexibility, has been successfully used in numerous academic studies, and contributes to numerical stability in the mathematical solution process.

$$v_{j} = \frac{\sum_{j=1}^{3} \left(\mu_{ij}^{m} X_{j}\right)}{\sum_{j=1}^{3} \left(\mu_{ij}^{m}\right)} = \frac{\mu_{i1}^{2} \Box_{l} + \mu_{i2}^{2} \Box_{2} + \mu_{i3}^{2} \Box_{3}}{\mu_{i1}^{2} + \mu_{i2}^{2} + \mu_{i3}^{2}} = \frac{0.49*8 + 0.04*0.6 + 0.01*0.05}{0.49 + 0.04 + 0.01} \cong 7,30$$
(15)

For a cluster with a determined center value  $(v_j)$ , the distances of the input vectors  $(x_j)$  from this center influence their degree of membership to the cluster. The centers of the other clusters determine to which cluster the data point is closer, and consequently, the degree of membership to that cluster. In the defuzzification process, fuzzy values are converted into precise numbers, such as the exact values of the PID parameters. During this process, the membership degrees and center values obtained from the fuzzy sets are taken into account, and the input vectors may be reprocessed accordingly. The input variables, such as error value(e(k)), change of error ( $\Delta$ e(k)), and oscillation level (Osc), are considered to play an important role in the adaptive behavior of the FCM-enhanced PID control system.

As shown in Tables 2, 3, and 4, MD (Medium Decrease), SD (Small Decrease), BD (Big Decrease), MI (Medium Increase), SI (Small Increase), and BI (Big Increase) represent the abbreviations for the fuzzy rule table outcomes. These rule bases for the PID parameters  $K_p$ ,  $K_i$ , and  $K_d$  are presented in Tables 2, 3, and 4, respectively. These three tables present the boundary values of the membership functions for e(k) [-7,-1, +1,+7],  $\Delta e(k)$  [-1.2,-0.2,+0.2 +1.2], and Osc [-2.5,-0.5,+0.5, +2.5]. Based on these boundary values, the fuzzy rule input values (SN, SP, BN, BP) are defined.

Table 2. FCM-PID fuzzy rule table for tuning the K<sub>p</sub> gain

e(k)	Δe(k)	Osc = BN	Osc = SN	Osc = SP	Osc = BP
BN	BN	MD	MD	MD	BD
BN	SN	MD	SD	SD	MD
BN	SP	MD	SD	SD	MD
BN	BP	BD	MD	MD	BD
SN	BN	SI	MI	MI	SI
SN	SN	SI	MI	BI	SI
SN	SP	SI	MI	MI	SI
SN	BP	SD	SI	SI	SD
SP	BN	SD	SI	SI	SD
SP	SN	SD	SI	SI	SD

SP	SP	MD	MI	BI	SD		
SP	BP	SD	MI	MI	SD		
BP	BN	BD	MD	MD	BD		
Table 2. FCM-PID fuzzy rule table for tuning the $K_p$ gain							
BP	SN	MD	SD	SD	MD		
BP	SP	MD	SD	SD	MD		
BP	BP	BD	MD	MD	MD		

Table 3. FCM-PID fuzzy rule table for tuning the  $\boldsymbol{K}_{i}$  gain

e(k)	Δe(k)	Osc = BN	Osc = SN	Osc = SP	Osc = BP
BN	BN	SD	SD	SI	SI
BN	SN	SI	SD	SI	SI
BN	SP	SI	SD	SI	SD
BN	BP	SD	SD	SI	MI
SN	BN	SD	SI	SI	SI
SN	SN	MD	SI	SI	SI
SN	SP	MD	SI	SI	SI
SN	BP	SD	SI	SI	SD
SP	BN	SD	SD	SI	SD
SP	SN	MD	SD	SI	SI
SP	SP	MD	SD	SI	SI
SP	BP	SD	SD	SI	SI
BP	BN	SD	SD	SD	MI
BP	SN	SI	SD	SD	SI
BP	SP	SI	SD	SD	SI
BP	BP	SD	SD	SD	MI

Table 4. FCM-PID fuzzy rule table for tuning the  $K_{\mbox{\scriptsize d}}$  gain

e(k)	Δe(k)	Osc = BN	Osc = SN	Osc = SP	Osc = BP
BN	BN	MI	BI	MI	SI
BN	SN	SI	BI	MI	SI
BN	SP	SI	MI	BI	SI
BN	BP	SI	MI	BI	MI
SN	BN	MI	MI	BI	SI
SN	SN	SD	SI	SI	SI
SN	SP	SD	SI	SI	MD
SN	BP	MI	MI	SI	SD
SP	BN	MI	SI	SI	SD

	SP	SN	SD	SD	MI	SD		
	SP	SP	SD	MD	BI	MD		
	SP	BP	MI	MI	MI	SD		
	Table 4. FCM-PID fuzzy rule table for tuning the $\rm K_{\rm d}$ gain							
	BP	BN	MI	MI	MI	MI		
	BP	SN	SI	MI	BI	SI		
	BP	SP	SI	BI	MI	SI		
•	BP	BP	MI	MD	MD	MI		
-								

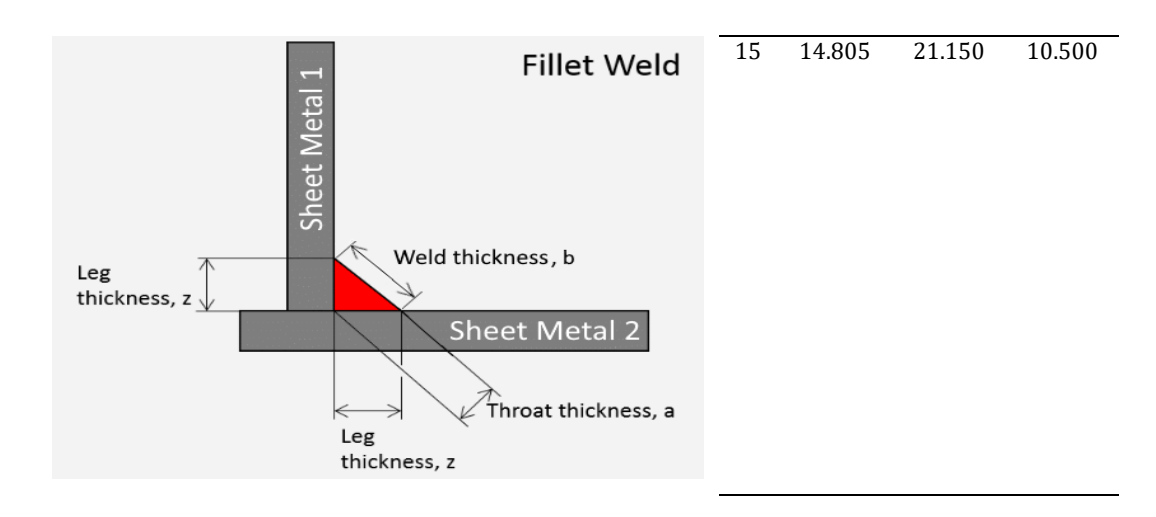
### F. Experimental Preparations and Welding Criteria

In this study, CLOOS brand QIROX QRC-350 model 6-axis welding robot and QIROX QC2 advanced model robot controller were preferred for conducting field studies for the Weld Guide experimental setup. Accordingly, a CLOOS Qineo 601 Pro welding machine with a 600 A capacity was utilized. Among these systems, the robot controller provides data communication between the devices via CANbus protocol, allowing the robot to optimize the welding seam tracking with real-time sensor feedback. During the field tests of this experimental setup, analog sensor data can be converted to 12-bit digital signals via an ADC built into the QC2 robot controller and processed in algorithms. The axes of the robot used in these experiments are controlled by servo motors with encoders that provide precise position and motion control. In the SH\_Qirox V09\_EN technical document prepared by CLOOS, it was learned that the position accuracy of the QRC-350 model is ±0.05 mm/m (50 microns). The accuracy of this robot when reaching a certain point is at a very high precision level for industrial robots. Thanks to this advantage, the accuracy of the data obtained in field studies with Weld Guide has increased significantly and the results have become more quantitative.

Deviations in weld seam tracking led to an extension of the free wire length. This leads to further thinning of the weld thickness. The suitability of this thickness value directly determines the mechanical strength and load-carrying capacity of the seam. In order to determine this suitability, various static analyses can be performed to examine the behavior of weld seams under static loads. According to ANSYS static analysis studies conducted in this context by selecting the Solid 186 element type, the minimum throat weld thickness in fillet welds of workpieces was determined by multiplying the thickness value of the thinner metal parts by a coefficient of 0.7 (Shyju et al., 2016). The accuracy of the ANSYS analyses is over 95% thanks to the mesh structure created in detail by providing appropriate factors. Considering this high accuracy, the same coefficient value was adopted for the weld thickness data in this paper.

Table 5. Minimum values according to sheet thickness in fillet weld

t	Z <sub>min(mm)</sub>	b <sub>min(mm)</sub>	a <sub>min(mm)</sub>
3	2.961	4.230	2.100
4	3.948	5.640	2.800
5	4.935	7.050	3.500
6	5.922	8.460	4.200
8	7.896	11.280	5.600
10	9.870	14.100	7.000
12	11.844	16.920	8.400



In this paper, the minimum weld criteria recommended for the fillet joint of two steel parts of thickness indicated by the symbol t are presented in millimeters in Table 5. In this table, Z stands for the weld throat thickness and b for the weld width. The minimum required values for 5 mm thick workpieces used during the welded experimental studies are shown in green fill in this table. With the help of the weld guide system, it will be discussed whether the values obtained in field tests are above the specified minimum thickness or not according to these quantitative data.

#### III. RESULTS AND DISCUSSIONS

#### A. Weld Guide System Test Results

In this paper, a study on the use of angle sensors in weld seam tracking is carried out. In this context, a comparative test was carried out with and without the use of the Weld Guide system. In this innovative system, angle sensors with spring return mechanisms are used as sensors. The mechanical stop in the spring mechanism of these sensors has adjustable features. In this way, by increasing the energy stored in the spring, it is a great advantage that the sensors can detect deviations faster and information can be accessed earlier.

QIROX QRC-350 model welding robot and QC2 model robot controller were used in the welding test studies for the Weld Guide system. Unlike conventional welding seam tracking systems, this system aims to minimize the amount of deflection of the welding torch by providing real-time feedback. As a result of the tests, it was possible to determine how much the deflection rate decreased and how much the weld thickness consistency improved when the Weld Guide system was used. These results show that the developed system has significant potential to improve precision in industrial welding applications.

In the first field test consisted of joining two ST52 specimens measuring 740x100x5 mm at an angle of 95 degrees using a linear welding process. In this seam tracking process, a deviation of 28 mm X-axis and 11 mm Y-axis was created relative to the starting point, as shown in Figure 9. This deviation was successfully detected by the Weld Guide system. By analyzing the change in angular measurements with the available probe arms, this system detected the error in the weld seam and guided the torch to the correct joint, as shown. The FCM-PID control method was employed to adaptively correct these deviations in real-time, adjusting the torch position based on the fuzzy clustering of error signals and PID-based corrective actions. In this test, the welding travel speed was set at 12 mm/s, and a mechanical welding caliper model 4835-1 from inside with a measurement accuracy (±10 microns) was used for the conformity of the weld seam. In these measurements, the weld seam, approximately 8 mm in thickness, was initiated after a welding travel of 43 mm and reached the seam center following a total welding travel of 62 mm within 5.7 seconds.

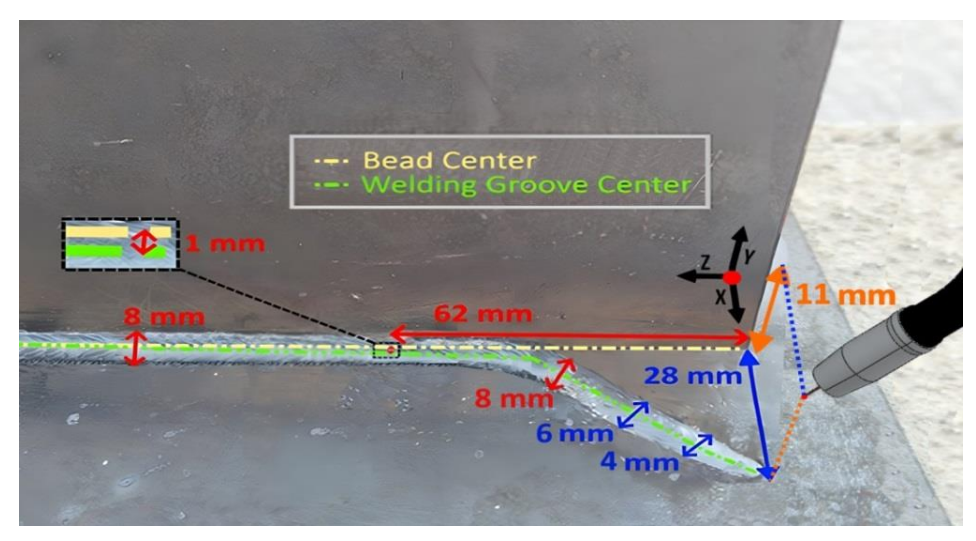


Figure 9. Tracking performance of a Weld Guide system in linear Seam Alignment using FCM-PID control

Following the initial welding tests, HAZ (Heat-Affected Zone) analyses enabled the acquisition of results at the microstructural level. In Figure 10 (a), when FCM-PID control was applied and the bead center was reached, the weld zone appears more uniform, indicating a more evenly distributed heat input. This results in greater penetration at the root and a wider HAZ, which is generally indicative of improved joint bonding and penetration quality. In contrast, in Figure 10 (b), where only conventional P control was used and the bead center was not accurately reached, the weld zone is narrower and exhibits an uneven distribution. These laboratory analyses highlighted the superior performance of the FCM-PID control in achieving consistent weld quality and enhanced seam characteristics.

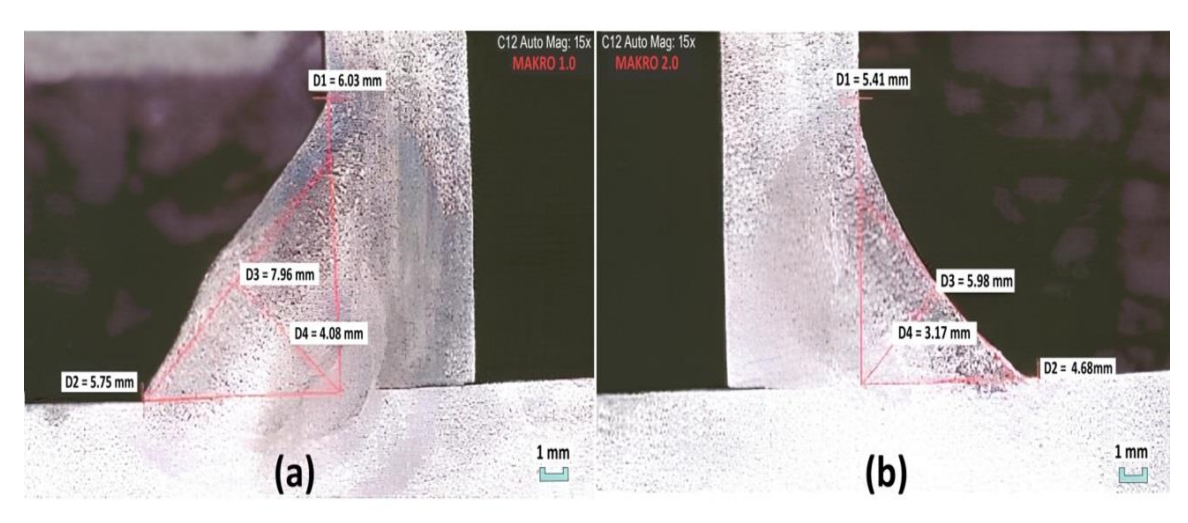


Figure 10. Comparison of HAZ at 62 mm of welding travel using (a) FCM-PID control, and (b) P control (Zeiss Axio Imager M2 optical microscope)

In the second field test involved the joining of two ST52 specimens measuring 620x85x5 mm at an angle of 85 degrees using a curvilinear welding process. In this seam tracking process, a deviation of 17 mm X-axis and 13 mm Y-axis was created relative to the starting point, as shown in Figure 11. This deviation was again accurately captured by the Weld Guide system as well. By analyzing the change in angular measurements with the available probe arms, this system detected the error in the weld seam and guided the torch to the correct joint as shown. The FCM-PID control method was employed to adaptively correct these deviations in real-time, adjusting the torch position based on the fuzzy clustering of error signals and PID-based corrective actions. In this test, the welding travel speed was set at 8 mm/s, and a mechanical welding caliper model 4835-1 was used for the conformity of the weld seam. In these measurements, the weld seam, approximately 8 mm in thickness, was initiated after a welding travel of 39 mm, and reached the seam center following a total welding travel of 35 mm within 4.8 seconds.

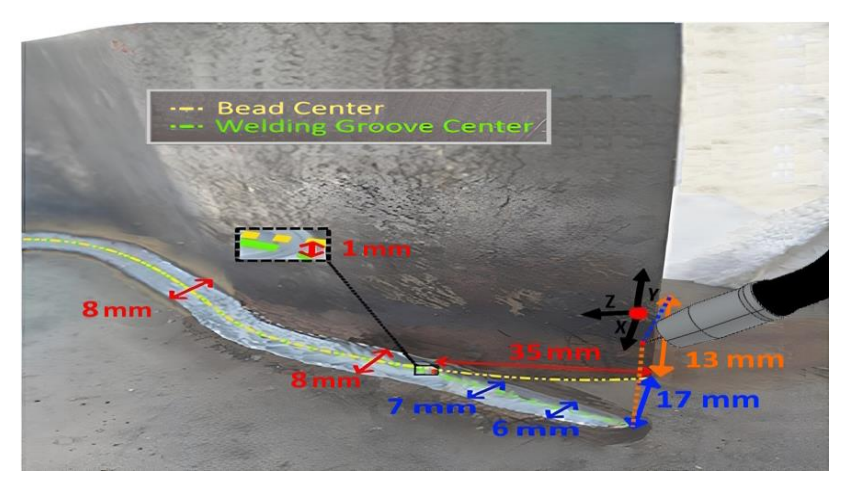


Figure 11. Tracking performance of a Weld Guide system in curvilinear Seam Alignment using FCM-PID control

All welding tests were conducted on ST52 steel, which limits the generalization of system behavior to materials with different surface characteristics. Detection accuracy may vary on highly vibratory or irregular surfaces, representing a critical parameter for field applications. The current system is compatible with MIG/MAG and SAW welding processes; however, integration with TIG and laser welding could enhance the system's industrial applicability. Such processes involve different arc characteristics and thermal distributions, potentially requiring a reconfiguration of the tracking algorithm. Additionally, during prolonged operations, continuous interaction of the sensor with the workpiece may lead to a gradual decrease in sensitivity, necessitating careful consideration of maintenance schedules and wear tolerances.

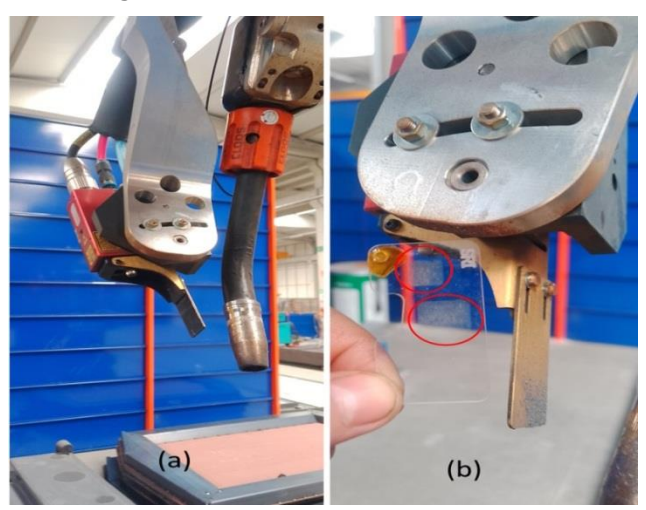


Figure 12. CLOOS robotic arm with a laser sensor (a), and protective glass for laser lenses exposed to contamination during welding (b)

In the third field test, we wanted to test the stable operation of the laser sensor with the QIROX QRC-350 robot shown in Figure 12 under harsh welding conditions. In this test, which was carried out under gas using a Qineo 601 Pro welding machine from CLOOS, two sample ST52 steel parts of 1500x95x4 mm were joined with a 75-degree fillet weld. Due to the large amount of spatter, a warning was received from the laser sensor at 80% of the test, and the welding process was stopped. When the test was resumed, another 20 mm was welded, and the failure was resumed. This was found to be caused by contamination on the protective glass, marked with a red circle in Figure 12. It was hypothesized that this adverse condition could be caused by excessive gas accumulation and high heat condensation due to the difficulty of free circulation of air in the restricted working zone. The laser sensor tends to misinterpret surface holes (particularly those larger than 3 mm) as seam features, causing the system to align toward them and resulting in substantial weld seam distortion, with deviations exceeding 7 mm. Experimental results confirmed that the Weld Guide system and the laser sensor can operate in conjunction, and both were successfully integrated into the welding torch. In cases of large deviations, the welding process was intentionally stopped, as failure to do so would compromise the accuracy and overall integrity of the welding operation.

The QRC2 robot controller stores the X, Y, and Z position information of the points numbered from 1 to 10,000 in the Point Editor interface. In the experimental studies, this coordinate information was rearranged according to the changes in the digital data sent by the Weld Guide system. In this context, the changes made to the interface while guiding the robot to the welding seam point are the parts shown in the red frame in Figure 13(a). In the robot controller shown in Figure 13(b), through the use of the developed text-based codes, the basic movements were changed and recorded within a 50-80 ms cycle time depending on the amount of error, change of error, and oscillation level. Likewise, thanks to the Search Procedure shown in the yellow frame, the coordinates required for the welding wire to reach the seam point again were successfully determined. This allowed the necessary corrections to be made for the corresponding process point number. The optimization was completed by saving the X -L, Y -L, and Z -L Cartesian movement points in the ROM memory of the Point Editor with the STORPOS command shown in the blue frame. In this context, the FCM-PID based Distinguish procedure was used to determine the TCP of the target point and to regulate the movements in the Cartesian axes. In this procedure, the deviation error in real-time TCP data in the X and Y axes is considered according to the Rule Base. Based on the fuzzy data, the Search Procedure (PROC SEARCH) was activated to find out which direction the robot should take.



Figure 13. The Point Editor interface in the QC2 Controller (a) and the code written in The Qirox Programming Language (b), which is similar to C Language

The sensor probe arm lengths of the Weld Guide system were measured as 92 mm for the first and 87 mm for the second. These probe arms start to rotate counterclockwise as long as they touch the edge of a workpiece. As a result of the tests, it was determined that the spring mechanism inside the RCB3100 sensors provides faster returns at angles of 14.8° and above. Therefore, the mechanical stops inside the sensor were changed from 2° to 15.7° for the first-angle sensor and 16.9° for the second-angle sensor. In the field welding tests, data was initially sent for these angle values, and these values started to increase from the moment of contact. For the linear welding test, when the weld seam point was reached, the mV data — corresponding to  $79.4^{\circ}$  for the first and  $61.7^{\circ}$  for the second — were used as the set values. In the curvilinear test, when the weld seam point was reached, the set values were determined as 55.8° for the first and 94.3° for the second. The set parameters were found to be appropriate with respect to the fillet weld angle. During realtime operation, the system was able to respond mechanically within 50–100 ms. In the RoboDK simulation, controller delays were incorporated using time sleep(ms) command to make the comparisons more realistic. The Weld Guide system performed contact measurements during a field test over a distance of 7 meters. The experiment was repeated 10 times, and upon completion of the tests, measurements were conducted using a Mitutoyo 293-821-30 digital micrometer. The evaluations revealed that the balls exhibited a maximum wear of 0.001 mm due to friction. Nevertheless, owing to the two high-hardness, heattreated bearing balls, the system was affected only at a negligible level by the surface wear. It was able to maintain its functionality without interruption.

In the fourth field tests for deviation improvement, the steady-state error, settling time, and overshoot were also measured in two field experiments conducted using three different control methods. The initial deviations in the curvilinear test were -16 mm for TCP X and -27 mm for TCP Y, welding travel speed 8

mm/s, and target deviation of 0.5 mm. Specifically, the results of curvilinear welding tests, illustrating the minimization of  $p_x$ , and  $p_y$  deviation values over time, are presented in Figure 14. In PID control, the deviation was reduced more quickly and stably compared to P control. Although the oscillations were lower than in P control, they were not completely eliminated. The total settling time was approximately 5.2 seconds based on a  $\pm 2$  % Settling Band. Thus, by incorporating past error information, the PID structure provided a more efficient approach to achieving equilibrium. In FCM-PID control, the shortest settling time of approximately 4.3 seconds was achieved. In these tests, the overshoot ratio in the FCM-PID controller was determined to be at the lowest level, within the range of 0.23 %, compared to classical PID and P control methods. Moreover, when compared with the other control strategies, the lowest steady-state error was measured at approximately 0.06 mm.

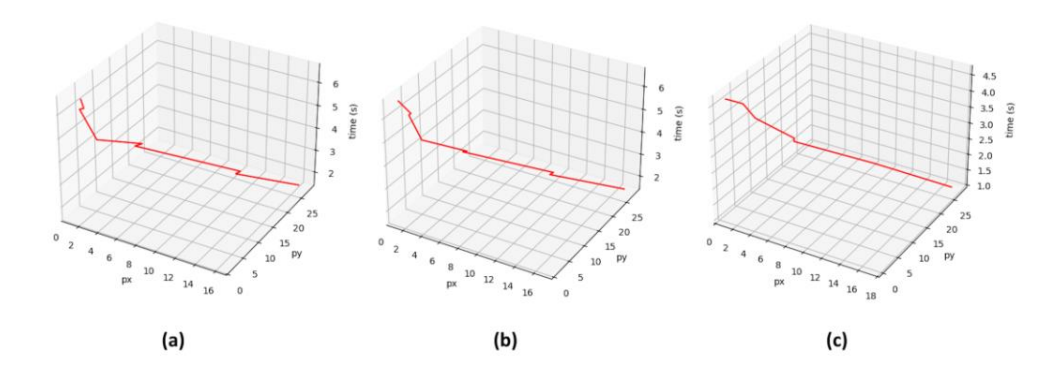


Figure 14. (a) Comparative optimization of weld seam tracking using P control, (b) PID control, and (c) FCM-PID control in curvilinear trajectories

In the fifth field test, the initial deviations were measured as -29 mm for TCP X and -22 mm for TCP Y. Correspondingly, the outcomes of linear welding tests, conducted at a welding travel speed (12 mm/s), and a target deviation of 0.5 mm. Specifically, the results of linear welding tests, illustrating the minimization of  $p_x$  and  $p_y$  deviation values over time, are depicted in Figure 15. In PID control, the deviation was reduced more quickly and stably, with oscillations being lower though not completely eliminated, resulting in a settling time of about 6 seconds. In contrast, the FCM-PID controller achieved the fastest response, reaching steady state in approximately 5 seconds based on a  $\pm 2$  % Settling Band. When the three graphs are compared, it is evident that the FCM-PID control method results in both reduced oscillations and a faster convergence to the desired outcome. Moreover, the overshoot in the FCM-PID controller was the lowest among the tested methods, measured at 0.28 %, compared to classical PID and P control. Additionally, the lowest steady-state error was recorded at approximately 0.08 mm when compared with the other control strategies.

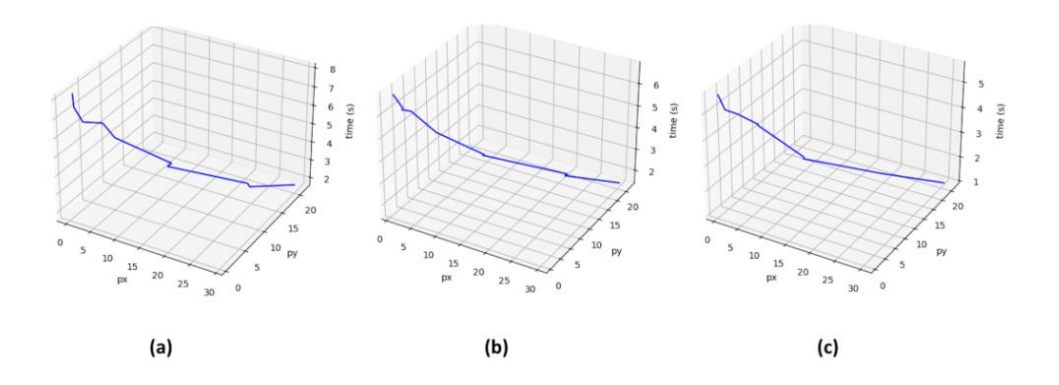


Figure 15. (a) Comparative optimization of weld seam tracking using P control, (b) PID control, and (c) FCM-PID control in linear trajectories

#### **B.** Discussion

Although the Weld Guide system demonstrated high accuracy with less than 0.6 mm deviation and approximately 98% consistency between simulation and field tests, particularly in simple, repeatable, and

easily measurable geometries, certain engineering limitations must be acknowledged. Mechanical wear, although measured as only 0.001 mm in the bearing balls after 7 m of continuous contact, may become more significant in long-term operations, especially under high-frequency ultrasonic welding, where vibrationinduced stresses accelerate material degradation. Additionally, the heat-affected zone (HAZ) during welding reaches 200-700 °C, which can lead to thermal expansion and microstructural deformations in contact components, potentially reducing measurement accuracy. The simulation environment (RoboDK) provided reliable kinematic verification but lacked realistic friction, force dynamics, and sensor noise modelling, which are critical for capturing nonlinear effects such as backlash or control-loop delays. To partially address this, random trajectory offsets (±0.1–0.12 mm) were introduced over 30 simulation runs, and combined RMS(Root Mean Square) error analysis showed an average positional error of ~ 0.07 mm/m for the CLOOS ORC-350 robot, consistent with its nominal repeatability. As mentioned before, according to the SH\_Qirox V09\_EN technical document prepared by CLOOS, it was indicated that the position accuracy of the QRC-350 model is ±0.05 mm/m. Additionally, controller delays have been incorporated into the simulations by including a time sleep of 50-100 ms, reflecting the delay time of the real control system. When these effects are also considered, taking into account all the capabilities of the current simulation program, the robot's trajectory motions are represented with an acceptable level of accuracy; however, incorporating additional physical effects could make the simulation more realistic

From an engineering perspective, the Weld Guide system may not fully replace advanced optical sensors under conditions with high reflectivity or surface irregularities. However, it offers a robust, low-cost, and wear-resistant alternative that provides reliable tracking in situations where camera- or laser-based systems often fail, such as in the presence of arc emission, spatter, or poor optical visibility. These findings clearly demonstrate the practical advantages of the Weld Guide system in industrial environments that require continuous operation and mechanical durability. Moreover, the system has significant horizontal scalability potential; to enable integration into large-scale applications across various industrial sectors, its operational scenarios should be diversified, and its adaptability to field conditions enhanced. Incorporating effects such as friction and sensor noise into simulations using MATLAB could have further strengthened the simulation framework.

#### IV. CONCLUSION

Welding processes may face quality issues in specific applications due to programming errors, high environmental temperatures, tolerance deviations in the workpiece, and irregularities arising from manufacturing. To minimize these problems and enhance the accuracy of the weld seam, studies are being conducted on advanced weld seam tracking systems. Laser sensor-based systems, which are widely utilized in the industry, are especially notable in applications requiring high precision and have a broad range of uses. However, a review of the existing literature reveals that laser sensor systems have certain limitations. It has been reported that, particularly with shiny surface workpieces, the radiation emitted by the melt pool formed in the weld zone distorts sensor data, leading to decreased measurement accuracy in deep weld gaps. Therefore, this study presents Weld Guide, an innovative mechanical guidance system capable of operating in particular with laser sensor systems or independently the weld seam tracking.

Comparison of simulation analyses with real field tests revealed that the obtained data exhibited a 98.1% consistency in trajectory, and the RoboDK simulation had a very low margin of error. This result indicates that advanced simulation software, such as RoboDK, can serve as an effective engineering tool in the design and verification processes of industrial robotic systems. In this experimental study, it was observed that deviations up to a maximum of 0.579 mm along the X and Y axes in the weld seam could be successfully detected using the Weld Guide system. This developed system proves to be a solution that offers high precision and reliability as an alternative to laser sensor source tracking systems that are expensive and frequently maintained in the field of industrial automation. The proposed system has demonstrated practical advantages in industrial environments where conventional optical sensors often fail.

In this study, the Weld Guide system developed was comparatively evaluated against conventional P and FCM-PID control methods, and quantitative results were obtained in terms of both the heat-affected zone (HAZ) characteristics and dynamic control performance. Microstructural analyses of the HAZ revealed that the FCM-PID control method enhanced thermal efficiency. Examinations performed with an optical microscope demonstrated that the application of FCM-PID control resulted in a wider and more homogeneous HAZ, with deeper penetration and improved joint strength. This finding demonstrates that the FCM-PID control provides significant improvements in the microstructural parameters directly

influencing weld quality, with a 28% increase in throat thickness and a 37% higher root penetration compared to conventional methods.

An analysis of the dynamic performance data revealed significant improvements in the positioning accuracy of the system. In the curvilinear welding test, with P control, the system exhibited a settling time of 6.43 s, an overshoot of 1.2%, and a steady-state error of 0.21 mm. With PID control, these values were reduced to 5.19 s, 0.33%, and 0.08 mm, respectively. In contrast, with FCM-PID control, the shortest settling time of 4.34 s was achieved, with an overshoot of only 0.23% and a steady-state error of 0.06 mm. This corresponds to reductions of 17.3% in settling time, 43.4% in overshoot, and 26.8% in steady-state error compared to PID control, respectively. Similarly, in the linear welding test, with P control, the settling time was 6.74 s, the over]. This was 1.3%, and the steady-state error was 0.26 mm. For PID control, these values improved to 6.02 s, 0.41%, and 0.10 mm, respectively. With FCM-PID control, the system reached steady state in 4.98 s, while the overshoot decreased to 0.28% and the steady-state error was reduced to 0.08 mm. This corresponds to reductions of 16.6% in settling time, 31.7% in overshoot, and 21.3% in steady-state error compared to PID control, respectively. These results demonstrate that the FCM-PID control not only minimized overshoot but also reduced steady-state errors, while achieving faster convergence compared to both classical P control and conventional PID control.

From an engineering perspective, these findings highlight that the Weld Guide system offers a significant alternative in industrial welding automation. Unlike conventional camera- and laser-based systems, which are severely affected by environmental factors such as intense arc radiation, surface perforations of larger than 3 mm in diameter, spatter contamination, and reflective surface conditions, the Weld Guide operates independently of such effects, thereby providing a cost-effective and durable solution. Moreover, the integration of FCM-PID-based optimization not only enhances accuracy through sensor feedback but also ensures high precision through intelligent control mechanisms

In future studies, several directions can be pursued to enhance and validate the Weld Guide system. One potential area is the integration of advanced machine learning techniques, including reinforcement learning or deep neural networks, to further improve decision-making, adaptability, and real-time correction capabilities. Expanding the applicability of the system to additional welding processes, such as TIG (Tungsten inert gas), ultrasonic, and laser welding, will help demonstrate its versatility. Moreover, incorporating multi-sensor fusion—combining optical, thermal, and mechanical feedback from angle sensors—can enhance measurement sensitivity and reliability, particularly in environments with high arc radiation or reflective surfaces. Additionally, long-term robustness studies under varying environmental conditions and with different workpiece materials will be essential to assess durability, consistency, and industrial applicability. In addition, by considering longer operating conditions, it would be possible to estimate how much time the wear on the contact balls may reach a critical level. Furthermore, the development of neural network- and PID-based hybrid system designs may contribute to providing the system with broader compatibility across different material types and welding techniques. Consequently, such improvements are expected to reduce error rates in the welding process, optimize manufacturing times and costs, and enhance efficiency and quality in industrial production processes. Furthermore, studies that focus on analyzing environmental effects, such as sensor noise and friction, within simulation environments—for example, MATLAB/Simulink—and comparing the results with experimental findings are expected to provide valuable insights.

#### **DECLARATIONS**

**Acknowledgements:** The authors would like to express their sincere thanks to the editor and the anonymous reviewers for their helpful comments and suggestions. The authors also acknowledge the support of ZETEST Quality Control Laboratory in Ankara for providing facilities for microstructural examinations. This study was conducted as part of a doctoral thesis entitled "Mechanical Feedback and Artificial Intelligence-Based Optimization in Robotic Welding."

**Author Contributions:** Conceptualization and methodology, A.D. and İ.A.Ö.; Control system contributions, A.D. and Z.Ö.; Writing—original draft preparation, A.D.; Writing—review and editing, İ.A.Ö. and Z.Ö. All authors have read and approved the final version of the manuscript.

**Availability of Data and Materials**: Data sharing is not applicable to this study.

**Conflict of Interest Disclosure:** A patent related to the Weld Guide system presented in this article (Registration No. 2023 012020) was granted to Selçuk University. The authors declare no other conflicts of interest.

**Copyright Statement:** The author(s) retain the copyright of their work published in the journal, which is licensed under the CC BY-NC 4.0 license, allowing others to share and adapt the work for non-commercial purposes with appropriate attribution

Funding/Supporting Organizations: This research received no external funding.

**Ethical Approval and Participant Consent:** This study does not involve human or animal participants. All procedures followed scientific and ethical principles, and all referenced studies are appropriately cited.

**Plagiarism Statement:** This article has been evaluated for plagiarism and no instances of plagiarism were detected.

**Use of AI Tools:** The author/authors declare that no Artificial Intelligence (AI) tools were used in the creation of this article.

#### REFERENCES

- Behrooz, F., Yusof, R., Mariun, N., Khairuddin, U., & Hilmi Ismail, Z. (2019). Designing intelligent MIMO nonlinear controller based on fuzzy cognitive map method for energy reduction of the buildings. *Energies*, *12*(14), Article 2713. https://doi.org/10.3390/en12142713
- Budde, L., Biester, K., Coors, T., Faqiri, M. Y., Lammers, M., Hermsdorf, J., & Overmeyer, L. (2023). Influence of shielding gas coverage during laser hot-wire cladding with high carbon steel. *The International Journal of Advanced Manufacturing Technology*, 127(7), 3195-3207. https://doi.org/10.1007/s00170-023-11350-z
- Bryn, O., Bekhta, P., Sedliačik, J., Forosz, V., & Galysh, V. (2016). The effect of diffusive impregnation of birch veneers with fire retardant on plywood properties. *BioResources*, *11*(4), 9112-9125. https://doi.org/10.15376/biores.11.4.9112-9125
- Canelas, A., Póvoa, R., Martins, R., Lourenço, N., Guilherme, J., Carvalho, J. P., & Horta, N. (2018). FUZYE: A Fuzzy c-Means Analog IC Yield Optimization Using Evolutionary-Based Algorithms. *IEEE Transactions on Computer-Aided Design of Integrated Circuits and Systems*, 39(1), 1-13. https://doi.org/10.1109/TCAD.2018.2883978
- Chao, C. T., Sutarna, N., Chiou, J. S., & Wang, C. J. (2019). An optimal fuzzy PID controller design based on conventional PID control and nonlinear factors. *Applied Sciences*, 9(6), Article 1224. https://doi.org/10.3390/app9061224
- Cibicik, A., Tingelstad, L., & Egeland, O. (2021). Laser scanning and parametrization of weld grooves with reflective surfaces. *Sensors*, *21*(14), Article 4791. https://doi.org/10.3390/s21144791
- Corke, P. (2017). Robot arm kinematics. In *Robotics, vision and control: Fundamental algorithms in MATLAB*® (2nd ed., pp. 193-228). https://doi.org/10.1007/978-3-319-54413-7\_7
- Costa, C. M., Veiga, G., Sousa, A., Rocha, L., Oliveira, E., Cardoso, H. L., & Thomas, U. (2018, April). Automatic generation of disassembly sequences and exploded views from solidworks symbolic geometric relationships. In *2018 International Conference on Autonomous Robot Systems and Competitions (ICARSC)* (pp. 211-218). IEEE. https://doi.org/10.1109/ICARSC.2018.8374185
- Elsisi, M., Zaini, H. G., Mahmoud, K., Bergies, S., & Ghoneim, S. S. (2021). Improvement of trajectory tracking by robot manipulator based on a new co-operative optimization algorithm. *Mathematics*, 9(24), Article 3231. https://doi.org/10.3390/math9243231
- Ferdaus, M. M., Anavatti, S. G., Garratt, M. A., & Pratama, M. (2019). Development of c-means clustering based adaptive fuzzy controller for a flapping wing micro air vehicle. *Journal of Artificial Intelligence and Soft Computing Research*, 9(2), 99-109. https://doi.org/10.2478/jaiscr-2018-0027
- Garbev, A., & Atanassov, A. (2020, October). Comparative analysis of RoboDK and robot operating system for solving diagnostics tasks in off-line programming. In *2020 International Conference Automatics and Informatics (ICAI)* (pp. 1-5). IEEE. https://doi.org/10.1109/ICAI50593.2020.9311332
- Haeri, H., Talehjerdi, A. G., Sarfarazi, V., Moayer, A., & Marji, M. F. (2024). A finite element analysis of the effects of TADAS dampers on the frame members' performances in concrete structures under Cyclic and monotonic loadings. *Iranian Journal of Science and Technology, Transactions of Civil Engineering*, 49(2), 1133-1156. https://doi.org/10.1007/s40996-024-01540-4

- Han, J., Shan, X., Liu, H., Xiao, J., & Huang, T. (2023). Fuzzy gain scheduling PID control of a hybrid robot based on dynamic characteristics. *Mechanism and Machine Theory*, 184, Article 105283. https://doi.org/10.1016/j.mechmachtheory.2023.105283
- Henriques, J. P. C., Neto, E. R., de Paula Paiva, J. P. M., de Souza, L. C., Lugli, A. B., Florentino, F. M., & de Andrade Carvalho, G. C. (2023, November). Trajectory generation using RoboDK for a Staubli SCARA TS 60 robot. In 2023 11th International Conference on Control, Mechatronics and Automation (ICCMA) (pp. 121-126). IEEE. https://doi.org/10.1109/ICCMA59762.2023.10374649
- Hong, L., Wang, B., Xu, Z., & Lv, D. (2018, August). Algorithm and application of inverse kinematics for 6-DOF welding robot based on screw theory. In 2018 International Conference on Information Technology and Management Engineering (ICITME 2018) (pp. 159-163). Atlantis Press. https://doi.org/10.2991/icitme-18.2018.32
- Huang, Y., Abu-Dakka, F. J., Silvério, J., & Caldwell, D. G. (2020). Toward orientation learning and adaptation in cartesian space. *Transactions on Robotics*, *37*(1), 82-98. https://doi.org/10.1109/TR0.2020.3010633
- Huynh, C. T., & Phung, T. C. (2024). Research on welding seam tracking algorithm for automatic welding process of X-shaped tip of concrete piles using laser distance sensor. *Robotica*, 42(6), 1796-1815. https://doi.org/10.1017/S0263574724000535
- Ibrahim, I. N., & Al Akkad, M. A. (2017). Studying the disturbances of robotic arm movement in space using the compound-pendulum method. *Bulletin of IzhSTU named after MT Kalashnikov, 20*(2), 156-159. https://doi.org/10.22213/2413-1172-2017-2-156-159
- Keles, A. E., Haznedar, B., Kaya Keles, M., & Arslan, M. T. (2023). The effect of adaptive neuro-fuzzy inference system (ANFIS) on determining the leadership perceptions of construction employees. *Iranian Journal of Science and Technology, Transactions of Civil Engineering*, 47(6), 4145-4157. https://doi.org/10.1007/s40996-023-01146-2
- Li, G., Hong, Y., Gao, J., Hong, B., & Li, X. (2020). Welding seam trajectory recognition for automated skip welding guidance of a spatially intermittent welding seam based on laser vision sensor. *Sensors*, 20(13), Article 3657. https://doi.org/10.3390/s20133657
- Li Sr, B., Qin, X., Lei, J., Zeng, Y., Zhang, J., Jia, B., Li, H., & Li, Z. (2021, November). Detection method of power line under uneven lightness for flying-walking power line inspection robot. In *Proceedings of the 2021 International Conference on Image, Video Processing, and Artificial Intelligence* (Vol. 12076, pp. 46-52). SPIE. https://doi.org/10.1117/12.2611653
- Lin, C. H., Wang, K. J., Tadesse, A. A., & Woldegiorgis, B. H. (2022). Human-robot collaboration empowered by hidden semi-Markov model for operator behaviour prediction in a smart assembly system. *Journal of Manufacturing Systems*, *62*, 317-333. https://doi.org/10.1016/j.jmsy.2021.12.001
- Liu, F., Wang, Z., & Ji, Y. (2018). Precise initial weld position identification of a fillet weld seam using laser vision technology. *The International Journal of Advanced Manufacturing Technology*, 99(5), 2059-2068. https://doi.org/10.1007/s00170-018-2574-9
- Lu, S., Zhou, J., & Zhang, J. (2015). Optimization of welding thickness on casting-steel surface for production of forging die. *The International Journal of Advanced Manufacturing Technology*, 76 (5), 1411-1419. https://doi.org/10.1007/s00170-014-6371-9
- Luo, J., Zhu, L., Wu, N., Chen, M., Liu, D., Zhang, Z., & Liu, J. (2022). Adaptive neural-PID visual servoing tracking control via extreme learning machine. *Machines*, 10(9), Article 782. https://doi.org/10.3390/machines10090782
- Morsi, N. M. (2024). *Feasibility testing of robotics inspection by advanced simulation for aerospace structures* (Doctoral thesis, Glasgow Caledonian University).
- Nguyen, H. C., & Lee, B. R. (2014). Laser-vision-based quality inspection system for small-bead laser welding. *International Journal of Precision Engineering and Manufacturing*, 15(3), 415-423. https://doi.org/10.1007/s12541-014-0352-7
- Petschnigg, C., Breitenhuber, G., Breiling, B., Dieber, B., & Brandstötter, M. (2018, March). Online simulation for flexible robotic manufacturing. In *Proceedings of the International Conference on Industrial Technology and Management* (pp. 88-92). IEEE. https://doi.org/10.1109/ICITM.2018.8333925
- Ramalingam, S., Rasool Mohideen, S., Manigandan, S., & Prem Anand, T. P. (2021). Hybrid polymer composite material for robotic manipulator subject to single link flexibility. *International Journal of Ambient Energy*, 42(5), 514-521. https://doi.org/10.1080/01430750.2018.1557551
- Reddy, J., Dutta, A., Mukherjee, A., & Pal, S. K. (2024). A low-cost vision-based weld-line detection and measurement technique for robotic welding. *International Journal of Computer Integrated Manufacturing*, *37*(12), 1538-1558. https://doi.org/10.1080/0951192X.2024.2314784
- Ružbarský, J. (2023). The difficulty of measuring the roughness of glossy surfaces using the triangulation principle. *Applied Sciences*, *13*(8), Article 5155. https://doi.org/10.3390/app13085155.

- Seefried, J., Mahr, A., Weigelt, M., Kühl, A., & Franke, J. (2021, December). Challenges of contacting processes for thin copper flat wires in the context of electromechanical engineering. In *Proceedings of the 2021 11th International Electric Drives Production Conference (EDPC)* (pp. 1-8). IEEE. https://doi.org/10.1109/EDPC53547.2021.9684202
- Sharkawy, A. N., & Khairullah, S. S. (2023). Forward and inverse kinematics solution of a 3-DOF articulated robotic manipulator using artificial neural network. *International Journal of Robotics and Control Systems*, *3*(2), 330-353. https://doi.org/10.31763/ijrcs.v3i2.1017
- Sharma, A., Sharma, K., Islam, A., & Roy, D. (2020). Effect of welding parameters on automated robotic arc welding process. *Materials Today: Proceedings, 26,* 2363-2367. https://doi.org/10.1016/j.matpr.2020.02.507
- Shyju, T., Saravanan, C., Kumar, T. S., & Kumaragurubaran, B. (2016). Static analysis of tube to header weld joint configurations. *International Journal of Engineering Research*, *5*(5), 440-446.
- Skála, J., Svantner, M., Tesar, J., & Franc, A. (2016). Active thermography inspection of protective glass contamination on laser scanning heads. *Applied Optics*, 55(34), 60-66. https://doi.org/10.1364/A0.55.000D60
- Soltani, A., & Vahidi Bajestani, A. (2024). Linear quadratic Gaussian control for a liquid-carrying quadrotor. *Iranian Journal of Science and Technology, Transactions of Electrical Engineering*, 48(1), 395-408. https://doi.org/10.1007/s40998-023-00657-y
- Suoranta, I. (2021). *Implementation of a laser sensor system in a multi-robot welding cell* (Master's thesis, LUT University, School of Mechanical Engineering). LUTPub. https://lutpub.lut.fi/handle/10024/162891
- Wang, B., Hu, S. J., Sun, L., & Freiheit, T. (2020). Intelligent welding system technologies: State-of-the-art review and perspectives. *Journal of Manufacturing Systems*, 56, 373-391. https://doi.org/10.1016/j.jmsy.2020.06.020
- Xue, K., Wang, Z., Shen, J., Hu, S., Zhen, Y., Liu, J., & Yang, H. (2021). Robotic seam tracking system based on vision sensing and human-machine interaction for multi-pass MAG welding. *Journal of Manufacturing Processes, 63,* 48-59. https://doi.org/10.1016/j.jmapro.2020.02.026
- Vacharakornrawut, N., Thepmanee, T., Rerkratn, A., & Pongswatd, S. (2016, June). Converting TCP to joints value of 6-DOF robot based on forward and inverse kinematic analysis. In 2016 13th International Conference on Electrical Engineering/Electronics, Computer, Telecommunications and Information Technology (ECTI-CON) (pp. 1-6). IEEE. https://doi.org/10.1109/ECTICon.2016.7561348
- Vocetka, M., Huňady, R., Hagara, M., Bobovský, Z., Kot, T., & Krys, V. (2020). Influence of the approach direction on the repeatability of an industrial robot. *Applied Sciences*, *10*(23), Article 8714. https://doi.org/10.3390/app10238714
- Vesović, M., Jovanović, R., & Zarić, V. (2024). Hybrid GA-ANFIS and PSO-ANFIS techniques for nonlinear DC motor system modeling. *Proceedings of the Institution of Mechanical Engineers, Part C: Journal of Mechanical Engineering Science*. https://doi.org/10.1177/09544062251350800
- Yang, L., Pan, Y., Liu, Y., Shang, Y., Yang, S., & Cao, H. (2020). Automatic guidance method for laser tracker based on rotary-laser scanning angle measurement. *Sensors*, *20*(15), Article 4168. https://doi.org/10.3390/s20154168
- Zhang, Z., Wan, Y., Wang, Y., Guan, X., Ren, W., & Li, G. (2021). Improved hybrid A\* path planning method for spherical mobile robot based on pendulum. *International Journal of Advanced Robotic Systems*, 18(1). https://doi.org/10.1177/1729881421992958
- Zou, Y., Wei, X., & Chen, J. (2020). Conditional generative adversarial network-based training image inpainting for laser vision seam tracking. *Optics and Lasers in Engineering*, 134, Article 106140. https://doi.org/10.1016/j.optlaseng.2020.106140